Pit-To-Crack Transition and Corrosion Fatigue of 12% Cr Steam Turbine Blade Steel

Bernd M. Schönbauer[1,*], Andrea Perlega[1], Stefanie E. Stanzl-Tschegg[1]

[1] Institute of Physics and Material Sciences, University of Natural Resources and Life Sciences, BOKU, Peter-Jordan-Str. 82, 1190 Vienna, Austria
* Corresponding author: bernd.schoenbauer@boku.ac.at

Abstract Several cases of undefined conditions during operation of steam turbines, such as shut down of the turbine or leaking of the condenser, can lead to a corrosive environment. If the concentration of oxygen and chloride exceeds a critical level, pitting corrosion can occur. Since corrosion pits increase the local stress field, the initiation of fatigue cracks is facilitated and – under adverse conditions – these cracks can lead to final failure.
In this work, the results of fatigue tests on 12% Cr martensitic stainless steel, which is a standard blade material in the low pressure part of a steam turbine, are presented. The influence of corrosion pits and environment on the fatigue limit is investigated. Pit-to-crack transition is studied by optical observation and fractographic examination. The test environments were air at 90 °C and an aqueous solution with defined content of chloride and oxygen. To simulate an aggressive environment in which corrosion pits can form, fatigue tests in aerated 6 ppm Cl^- solution at 90 °C are performed.

Keywords Corrosion Fatigue, Pitting Corrosion, Very High Cycle Fatigue, Kitagawa Diagram, 12% Cr Steel

1. Introduction

Failure of steam turbines often takes place at the last stage of the low pressure blades where early condensate occurs. Although steam turbines were designed for a maximum operational time of 20 years, several turbines are in service since more than four decades. The turbine blades are loaded by different kinds of stresses. High mean stresses due to centrifugal forces and superimposed cyclic loading with low stress amplitudes induced by inhomogeneous steam flow with load frequencies of ca. 2 kHz are acting. Therefore, fatigue life data for high stress ratios in the very high cycle fatigue (VHCF) regime are important to predict fatigue life. Fatigue cracks were frequently observed to initiate at corrosion pits. During standard operational conditions the absence of impurities – such as chlorides – and oxygen prevents the material from corrosion. But shut down of the turbine or leaking of the condenser leads to undefined conditions where corrosion pitting may occur. Martensitic 12% Cr steel is a standard material for blades in the low pressure part of steam turbines. Extensive research was started already in the 1980s to simulate and understand the phenomenon of corrosion assisted fatigue of blading materials [1,2]. A project with the aim to develop a methodology for the prediction of corrosion fatigue life in steam turbine blades is still in progress [3] and several results were already presented [4-7].
In the present work, fatigue life test results are presented for smooth and pre-pitted specimens. The influence of stress range R and pit dimension is discussed for different environments. Fatigue tests were performed at 90 °C in air and aqueous solution. De-aerated 300 ppb Cl^- solution is often used to simulate service conditions in the low pressure part of steam turbines where early condensate occurs [8]. Since fatigue life tests in de-aerated solution and air lead to similar results [5], only the data determined in air are discussed in this work. To simulate a more aggressive environment in which corrosion pits may form, additional tests in aerated 6 ppm Cl^- solution at 90 °C were carried out. Crack initiation at corrosion pits was investigated by optical observation during fatigue loading. The fatigue crack growth rates (FCGRs) were determined and compared to measurements of long crack growth [7]. Fractographic examinations with scanning electron microscope (SEM) were performed in order to investigate crack initiation mechanisms.

2. Materials and experimental procedure

2.1. Material

The investigated material is a dual certified 403/410 martensitic 12% Cr steel. The material was hardened at 913 °C and tempered. The chemical compositions and the mechanical properties (provided by the supplier) are listed in Table 1 and 2. The mean grain size was 6 µm.

Table 1. Chemical composition of 403/410 SS (in weight %)

C	Cr	Mn	Si	Ni	Mo	Cu	S	P
0.13-0.14	11.79-11.8	0.41-0.49	0.18-0.26	0.28-0.33	0.13-0.18	0.07-0.10	<0.002	<0.020

Table 2. Mechanical Properties of 403/410 SS at room temperature

Tensile Strength (MPa)	Yield Strength (MPa)	Elongation (%)	Reduction of Area (%)
767	596	23	68

2.1. Test specimens

The shape of the test specimen for fatigue life tests is shown in Figure 1a. The specimens were machined, ground and polished with abrasive paper (up to grade #4000). The obtained mirror-like finish enabled observation of fatigue cracks that initiated at corrosion pits. To eliminate residual stresses, the specimens were stress-relief annealed in high vacuum (10^{-6} Pa). The stress relief procedure was: Heating from room temperature to 600 °C 1 h, holding for 2 h, cooling from 600 °C to 400 °C in 2 h and to room temperature in approx. 12 h. Additional specimens were produced with corrosion pits located in the gauge length of the specimen. A typical corrosion pit on the surface of a test specimen is shown in Figure 1b. The pre-pitting procedure was developed and arranged at the National Physical Laboratory and is described in more detail in [9]. Corrosion pits with depths of ca. 50, 100 and 250 µm were used. The actual depths were ±10% of the targeted value.

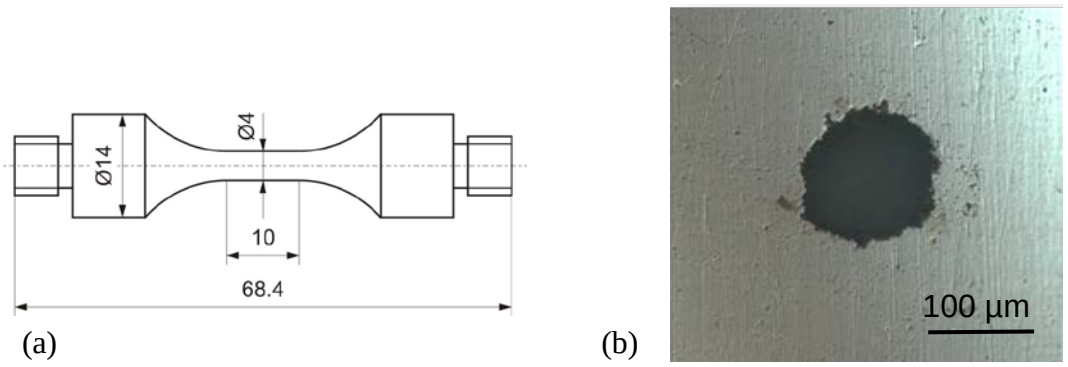

(a) (b)

Figure 1. Specimen shape for fatigue life tests (a) and corrosion pit in the gauge lengths of the specimen (b)

2.2. Fatigue testing method

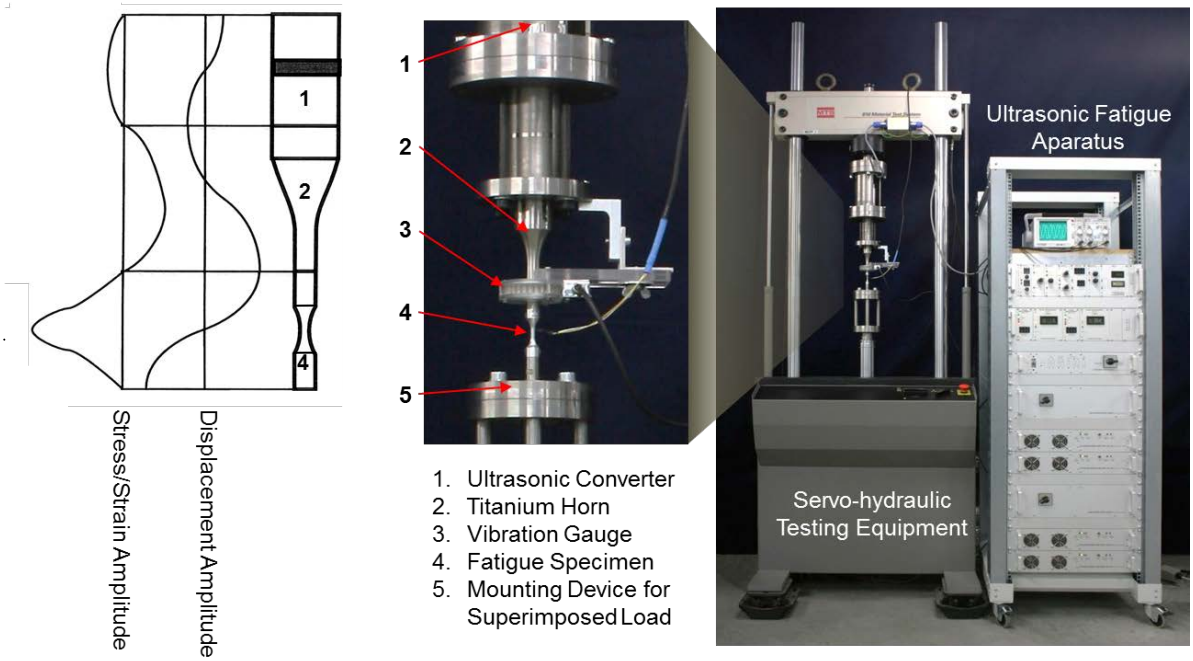

Figure 2. Ultrasonic fatigue test setup

The fatigue tests were conducted with an ultrasonic fatigue testing equipment. The ultrasonic converter is attached to a servo-hydraulic testing equipment which allows testing at higher stress ratios by superimposing static loads. The ultrasonic fatigue technique works by stimulating specimens to resonance vibration. The geometry of the resonance system – including the test specimen – is adjusted to achieve a resonance frequency of approximately 20 kHz. The failure location (region with maximum stress/strain amplitude) is stationary and therefore can be observed optically during fatigue testing. This is due to the absence of a vibration amplitude at the node of the standing wave during oscillation. An optical system with 250x magnification was used to detect crack elongations of less than 10 µm.

2.3. Aqueous solution circulation system

A water circulation loop with a 35-l-reservoir was used for measurements in aqueous environments. The set-up is shown schematically in Figure 3 and described in more detail in [7]. It allows testing in solutions with defined content of chloride and oxygen at constant temperature. Aeration was achieved by passing laboratory air with a diaphragm pump into the solution. Conductivity and oxygen level were detected during measurement. The flow rate of the liquid was 3 l/hour. The corrosion potential was measured using an Ag/AgCl reference electrode but the potentials quoted are referred to the saturated calomel electrode (SCE) at 25 °C. The corrosion potential during fatigue testing in aerated 6 ppm Cl^- solution was between -0.18 V(SCE) and 0.01 V(SCE).
Ultrapure water (initial conductivity of 0.06 µS/cm and AR grade NaCl) was used to prepare the solution. A new solution was used whenever the conductivity of the water increased by 10% of the initial value.

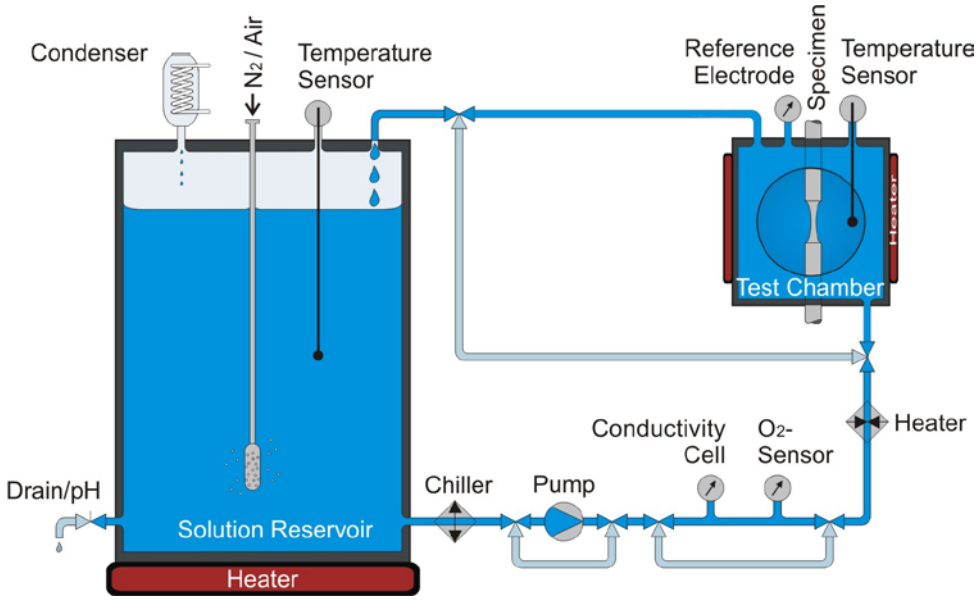

Figure 3. Schematic of the aqueous solution circulation system

3. Results

S-N tests were performed on smooth and pre-pitted specimens with pit depths of 50, 100 and 250 µm. The fatigue limit $\Delta\sigma_0$ was defined as the cyclic stress range where at least two specimens survived a minimum of 1×10^9 cycles. Specimens that did not fail – so called run-outs – are marked with arrows in the *S-N* plots. The fracture surfaces were observed by scanning electron microscopy (SEM).
The dimensions of the pits were determined from the fracture surface. The maximum variability in pit depth was defined to be ±10% of the proposed size. 55 pre-pitted specimens met that requirement and are plotted in *S-N* diagrams. To enable measurement of the run-out specimens with corrosion pits, they were loaded at higher stress ranges until failure occurred.

3.1. Fatigue lives in air at 90 °C

Results of the *S-N* tests in air at 90 °C are shown in Figure 4a. A significant decrease of the fatigue limit $\Delta\sigma_0$ with increasing stress ratio and pit size is obvious.
The determined fatigue limits $\Delta\sigma_0$ are plotted in a Haigh diagram where the stress amplitude $\Delta\sigma/2$ is plotted versus the mean stress σ_m, see Figure 4b. For both, smooth and pre-pitted specimens, the results can be fitted by Gerber parabolas:

$$\Delta\sigma_0 = \Delta\sigma_{0,R=-1} \cdot (1 - \sigma_m/\sigma_u)^2). \quad (1)$$

Since the fatigue limits at fully reversed loading ($R = -1$) $\Delta\sigma_{0,R=-1}$ (which is equivalent to the values at the ordinate in the Haigh diagram) were not determined, the values were obtained by extrapolation of the curves. Both the determined fatigue limits and the assumed values for $R = -1$ are summarised in Table 3.

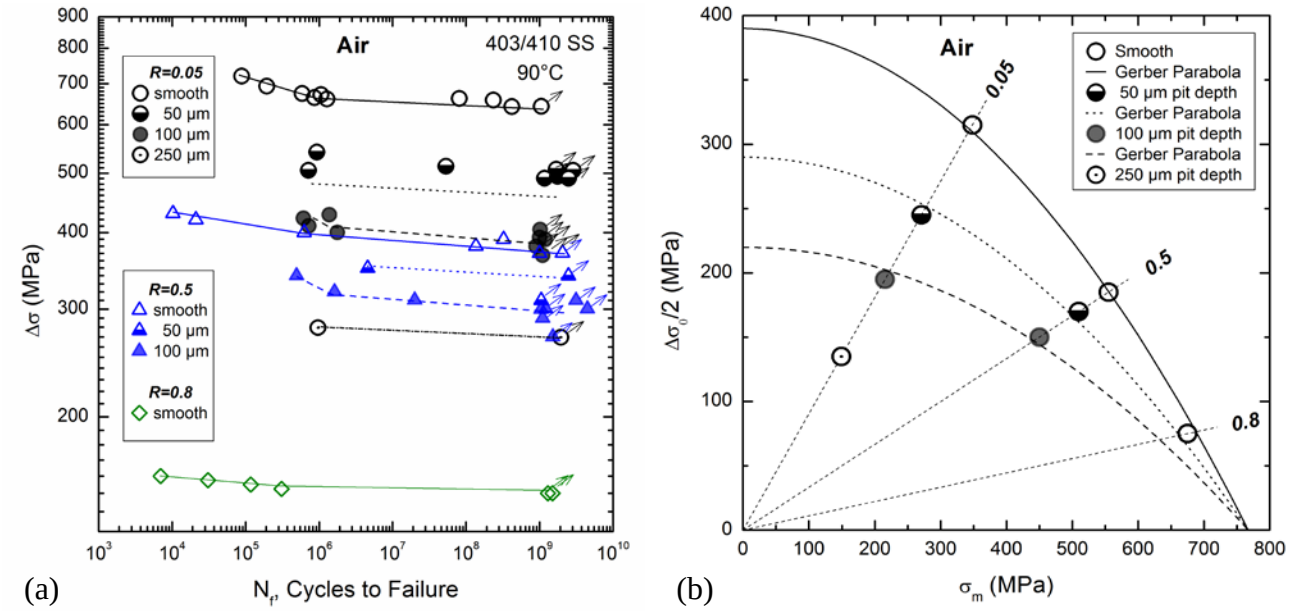

Figure 4. *S-N* plot (a) and Haigh diagram (b) for smooth and pre-pitted specimens in air at 90 °C

Table 3. Fatigue limits determined in air at 90 °C (in MPa)

Pit size	R = 0.05	R = 0.5	R = 0.8	R = −1*
Smooth	630	370	150	780
50 µm	490	~340	-	580
100 µm	390	300	-	580
250 µm	~270	-	-	-

* stress ranges for R = −1 obtained by extrapolation

3.2. Fatigue lives in aerated 6 ppm Cl^- solution at 90 °C

Results of the *S-N* tests in aerated 6 ppm Cl^- solution at 90 °C are shown in Figure 5a. The fatigue limits are again plotted in a Haigh diagram (Figure 5b) and summarised in Table 4. The Gerber parabola according to Eq. 1 fits well for smooth specimens. But for pre-pitted specimens, the deviation from the parabola is higher.

Table 4. Fatigue limits determined in aerated 6 ppm Cl^- solution at 90 °C (in MPa)

Pit size	R = 0.05	R = 0.5	R = 0.8	R = −1*
Smooth	530	330	145	600
100 µm	350	220	~130	320
250 µm	-	-	105	

* stress ranges for R = −1 obtained by extrapolation

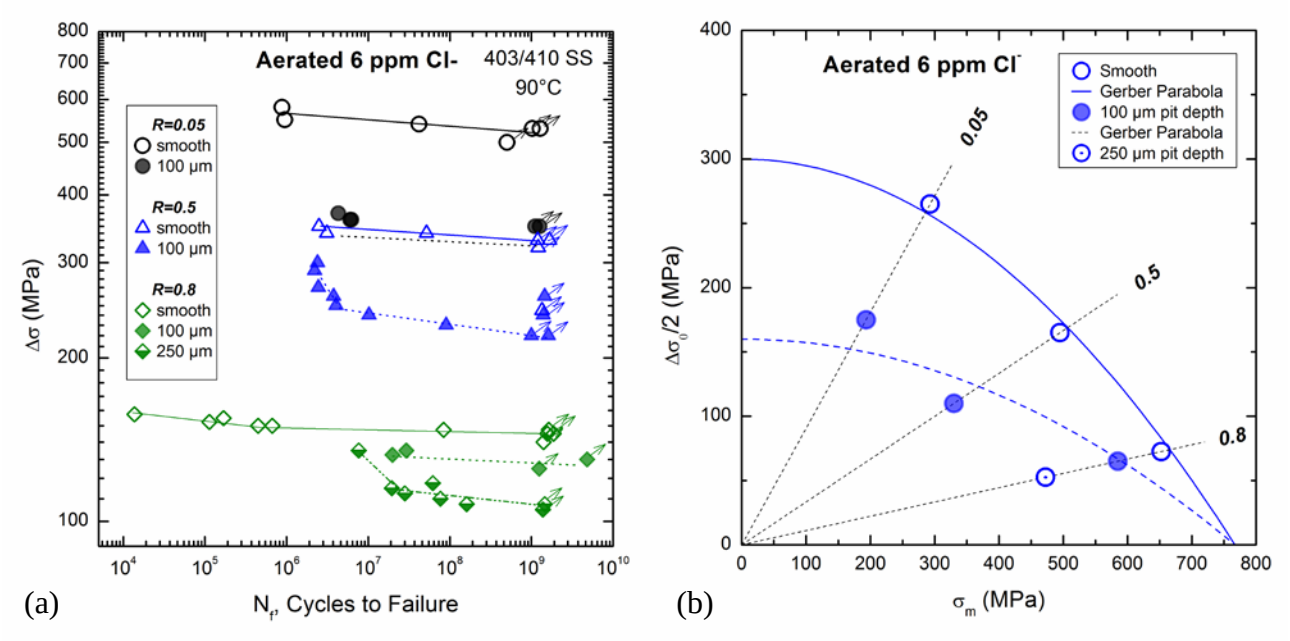

Figure 5. *S-N* plot (a) and Haigh diagram (b) for tests in 6 ppm Cl^- solution at 90 °C

3.3. Pit-to-crack transition

Pit-to-crack transition was observed by optical observation of the pit during fatigue loading. FCGRs were determined by measuring the crack extension during fatigue loading. The applied stress range was kept constant during testing which consequently increased the stress intensity factor range with crack elongation. Cracks were observed at stress ranges below the fatigue limit of pre-pitted specimens that initiated during fatigue loading but became non-propagating. The stress intensity factor range was calculated assuming a semi-circular crack shape. Figure 6a shows the FCGR curves for cracks emanating from pits with depths of 50 µm and 100 µm. For each pit size, the growth rates of a crack that caused final failure and one that became non-propagating are shown.

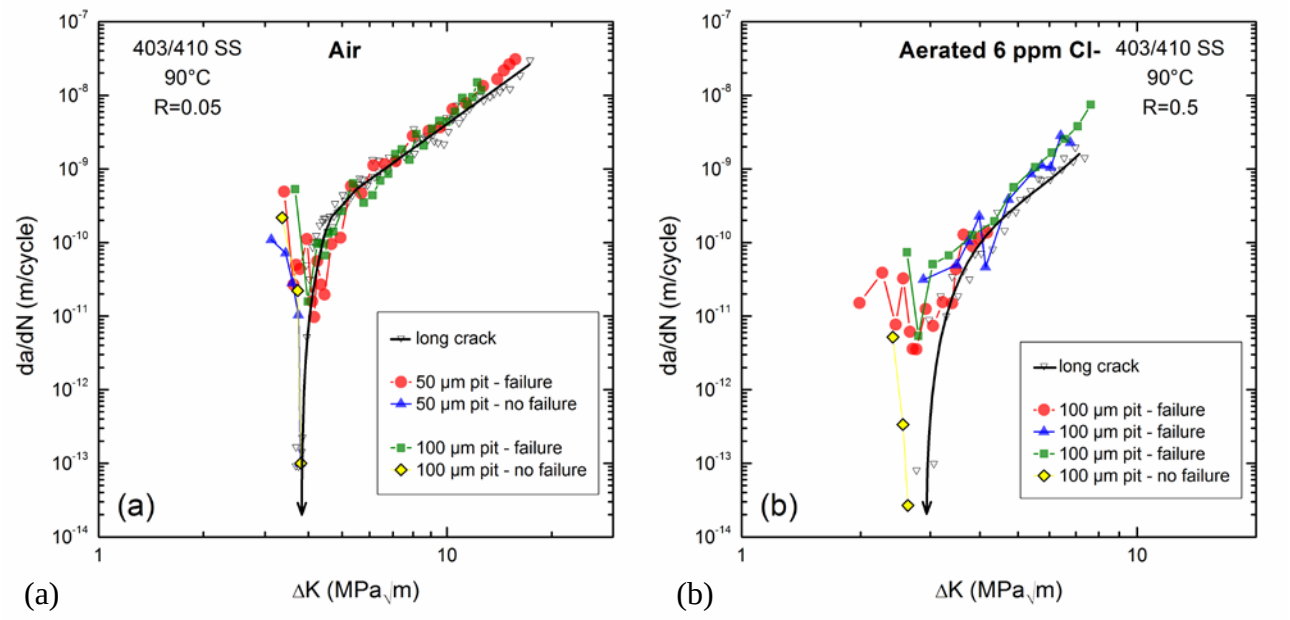

Figure 6.d*a*/d*N* vs. Δ*K* for cracks emanating from corrosion pits in: air (a) and aerated 6 ppm Cl^- solution (b)

The same is shown in Figure 6b for measurements in 6 ppm Cl^- solution. The FCGR curves are compared with long crack growth rate curves of the same material [3,7]. The cracks that initiated at the pits show the typical short-crack behaviour of crack elongation at stress intensities below the threshold. These cracks either arrest at microstructural barriers or progress and become long cracks. This behaviour was found for both environments as can be seen in Figure 6 although the calculated stress intensities for cracks that initiated at pits are only a rough estimation.

3.4. Fractography

3.4.1. Fatigue tests in air at 90 °C

Observation of the fracture surfaces with SEM and optical microscope gave information about crack initiation site and mechanisms. At $R = 0.05$, the smooth specimens failed from surface inclusions as shown in Figure 7a. Analysis with EDX identified these non-metallic inclusions with diameters of approx. 10 µm as Al_2O_3. Two specimens that failed during testing in air after 10^8 cycles failed from the interior. A so called fish-eye fracture was found. Crack initiation was in the matrix, and no inclusion could be detected.

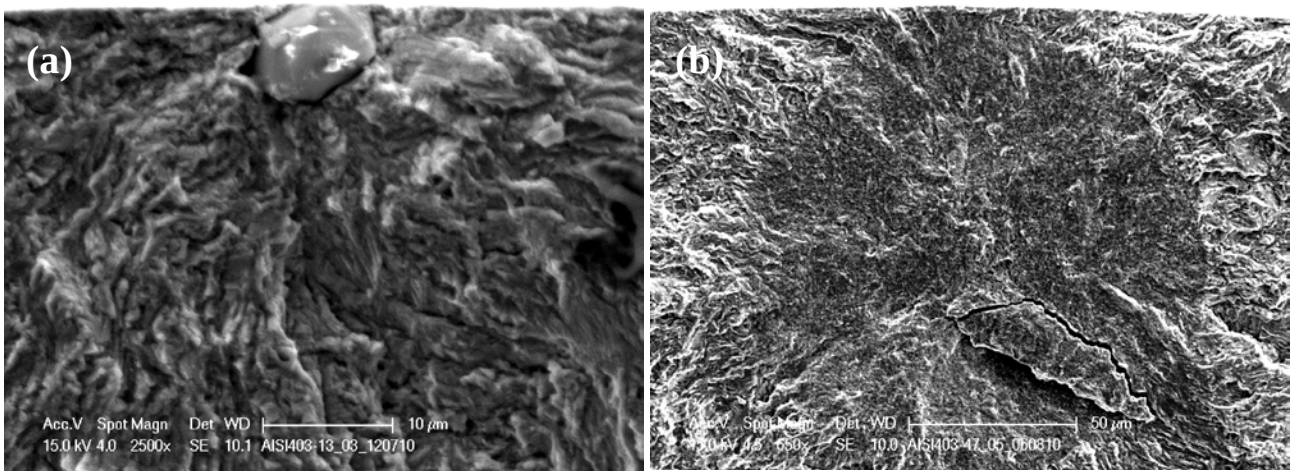

Figure 7. Fracture surfaces of smooth specimens tested at $R = 0.05$ in air at:
$\Delta\sigma = 672$ MPa ($N_f = 1.06 \times 10^6$) (a) and $\Delta\sigma = 642$ MPa ($N_f = 4.20 \times 10^8$) (b)

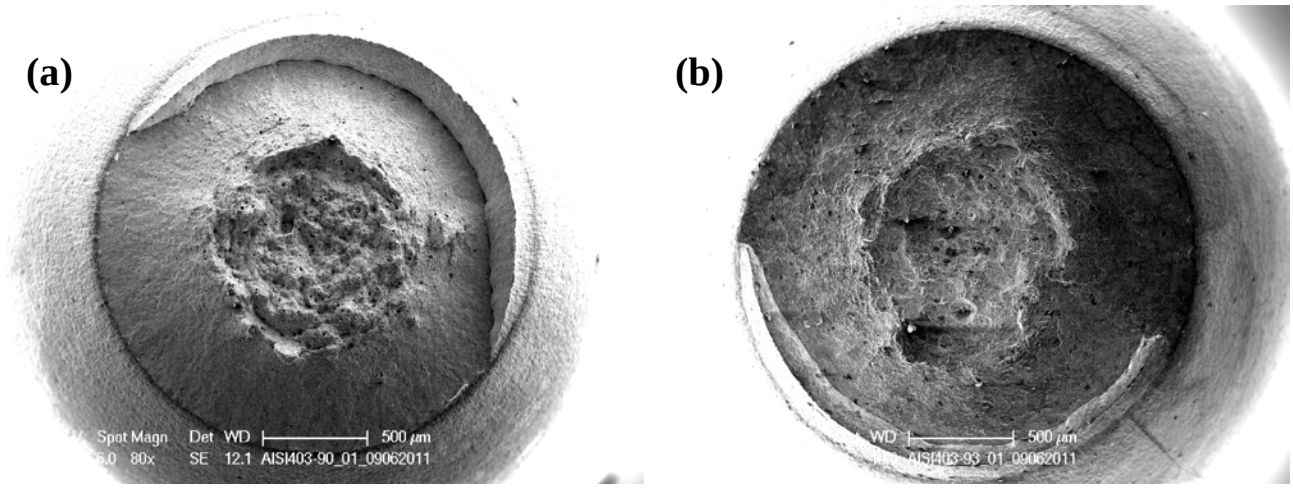

Figure 8. Fracture surfaces of smooth specimens tested at $R = 0.5$ in air at:
$\Delta\sigma = 380$ MPa ($N_f = 1.36 \times 10^8$) (a) and $\Delta\sigma = 400$ MPa ($N_f = 6.25 \times 10^5$) (b)

At $R = 0.5$ and $R = 0.8$, the crack initiation site for smooth specimens is not detectable since very high deformation at the fractured surface was observed. The cup-and-cone fracture as shown in Figure 8a and b was found for all smooth specimens. This kind of fracture surface is usually observed after tensile testing and suggests the dominance of cyclic creep due to the high maximum stress. Cyclic softening of the material during testing is supposed as reported by Kovacs et al. [10] for 12% Cr steel martensitic steel (X10CrNiMoV12-2-2). Nevertheless, failure occurred above 10^8 cycles.

For pre-pitted specimens tested at $R = 0.05$, crack initiation was always found at the pit. Figure 9 shows corrosion pits of different depths at the crack initiation sites. But at higher stress ratios, corrosion pits need not necessarily cause final failure. At $R = 0.5$, one of three pre-pitted specimens with a pit depth of ca. 50 µm showed high plastic deformation and a short crack after fatigue failure (Figure 10a). The corrosion pit was found some millimetres away from the fractured surface and the fracture was cup-and-cone like (Figure 10b). Similarly, short cracks were found at 100 µm deep pits when they were tested at $R = 0.8$ but none of these caused final failure. This means that there is a critical pit size depending on the stress ratio which may cause final failure. A greater pit size leads to a lower fatigue limit. Consequently, cyclic creep becomes an opposing mechanism when the maximum stress – i.e. the stress ratio – is higher. If the pit is rather small, high stresses are necessary to initiate a fatigue crack, and the material shows cyclic softening.

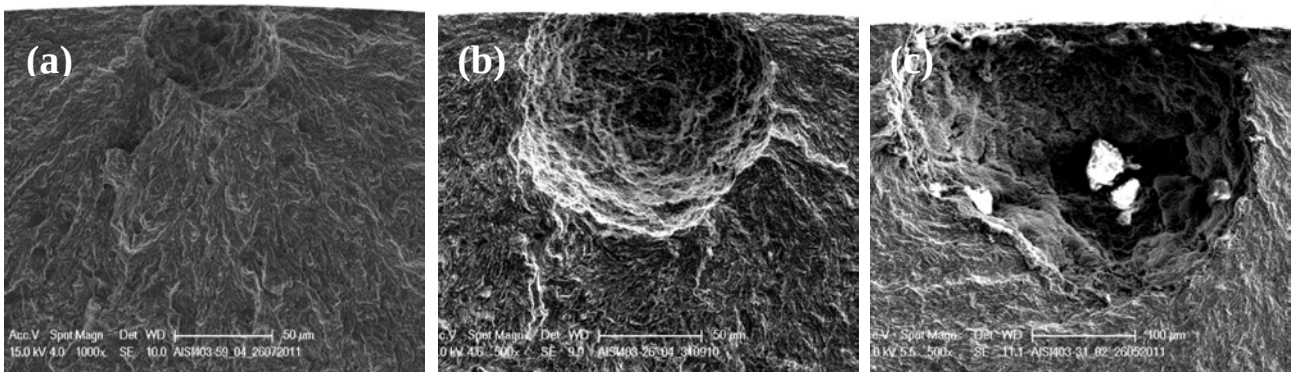

Figure 9. Fracture surfaces of pre-pitted specimens tested at $R = 0.05$ in air with a pit depth of: 50 µm ($\Delta\sigma = 507$ MPa, $N = 1.69 \times 10^9$) (a), 108 µm ($\Delta\sigma = 422$ MPa, $N_f = 6.11 \times 10^5$) (b) and 277 µm ($\Delta\sigma = 280$ MPa, $N_f = 9.65 \times 10^5$) (c)

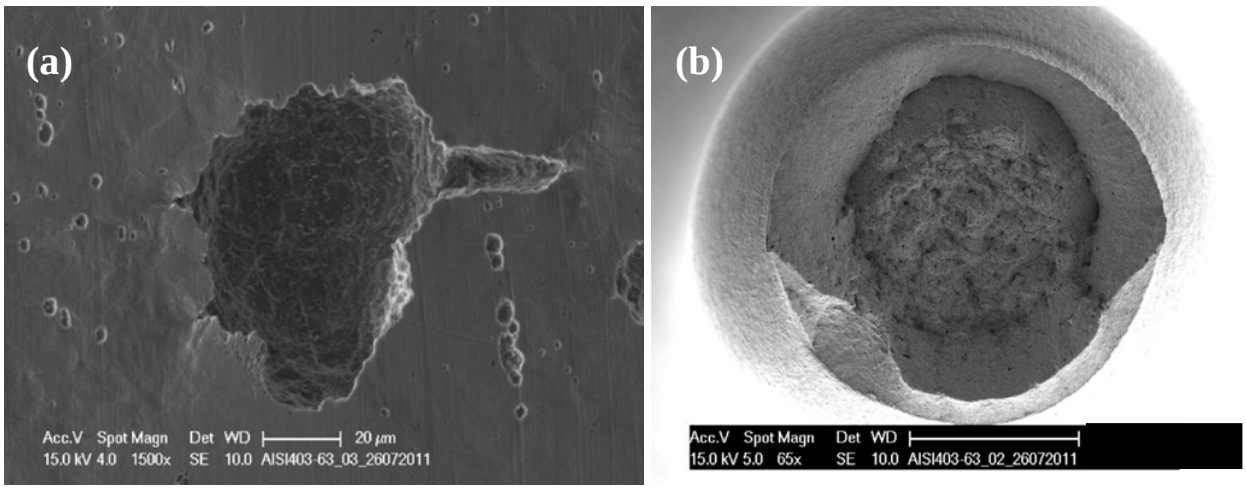

Figure 10. Corrosion pit with a depth of 48 µm (a) and fracture surface (b) of a specimen tested at $R = 0.5$ at $\Delta\sigma = 651$ MPa ($N_f = 2.38 \times 10^8$)

2.4.2. Fatigue tests in aerated 6 ppm C^- solution at 90 °C

S-N tests with smooth specimens showed a similar crack initiation behaviour like tests in air. Al_2O_3 inclusions were found again at the crack initiation site. Due to the decrease of the fatigue limit in the corrosive liquid, the cup-and-cone like fracture caused by cyclic creep was found only for tests at $R = 0.8$. Figure 11a shows a smooth specimen that was fatigue loaded at $R = 0.5$. An Al_2O_3 inclusion is located at the crack initiation site. Also the critical pit size for causing final failure at higher stress ratios is reduced. All pre-pitted specimens that were tested in the solution showed failure emanating from the pit. A corrosion pit with a depth of 100 µm is shown on the fracture surface of a specimen tested at $R = 0.8$ in Figure 11b.

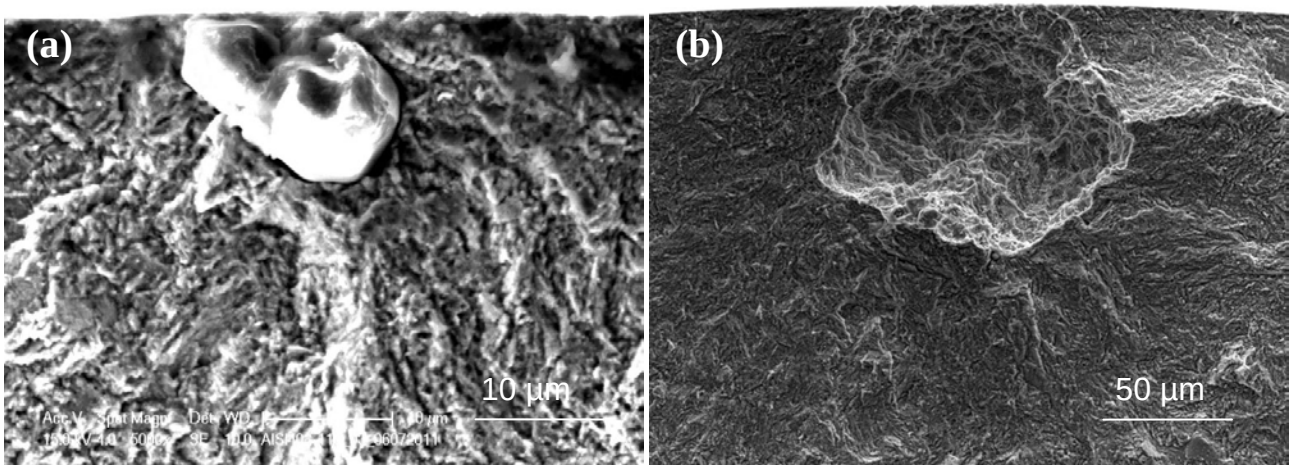

Figure 11. Fracture surfaces after testing in aerated 6 ppm Cl^- solution: smooth specimen at $R = 0.5$ ($\Delta\sigma = 340$ MPa. $N_f = 3.11 \times 10^6$) (a) and 101 µm deep pit at $R = 0.8$ ($\Delta\sigma = 135$ MPa, $N_f = 2.93 \times 10^7$) (b)

Acknowledgements

The presented results were achieved during a program to develop a methodology for the prediction of corrosion fatigue life in steam turbine blades, being conducted by the Electric Power Research Institute (EPRI) of Charlotte NC.

References

[1] EPRI. Proceedings of *Corrosion Fatigue of Steam Turbine Blade Materials*, R.I. Jaffe (Ed.), 21-24 Sept. 1981, Palo Alto, Ca, Pergamon Press, New York Oxford Toronto Sydney Frankfurt Paris, (1983).

[2] *Corrosion Fatigue of Steam Turbine-Blading Alloys in Operational Environments*. EPRI, Final Report CS-2932: 1984.

[3] *Program on Technology Innovation: Development of a Corrosion-Fatigue Prediction Methodology for Steam Turbines, Test Results of 12% Cr Blade Steel (403/410SS).* EPRI, Final Report 1023196: 2012.

[4] B. Schönbauer, S. Stanzl-Tschegg, N. Rieger, R. Salzman, A. Turnbull, S. Zhou and D. Gandy, *Crack Initiation and Propagation in 12% Cr Steam Turbine Blade Steel*. Proceedings of *VHCF5*, 28-30 June 2011, Berlin, (2011) pp. 545-550.

[5] B. Schönbauer, A. Perlega, S. Tschegg, N. Rieger, R. Salzman and D. Gandy, *Influence of*

Corrosion Pits and Environment on the Fatigue Life of 12% Cr Steam Turbine Blade Steel. Proceedings of *ICMFM-XVI*, 24-26 Sept. 2012, Brno, (2012) pp. 25-32.

[6] B. Schönbauer, S. Stanzl-Tschegg, N. Rieger, R. Salzman and D. Gandy, *Influence of Corrosion Pits on the Fatigue Limit of 12% Cr Steam Turbine Blade Steel*. Proceedings of *ECF 19*, 26-31 Aug. 2012, Kazan, (2012).

[7] B.M. Schönbauer and S.E. Stanzl-Tschegg, *Influence of Environment on the Fatigue Crack Growth Behaviour of 12% Cr Steel.* Ultrasonics (Ultrasonic Fatigue of Advanced Materials) (2013).

[8] S. Zhou and A. Turnbull, *Steam Turbine Operating Conditions, Chemistry of Condensates and Environment Assisted Cracking - An Overview*. NPL, Report MATC (A) 45: 2002.

[9] *Corrosion-Fatigue Prediction Methodology*. EPRI, Report EP-P31022/C14387: 2009.

[10] S. Kovacs, T. Beck and L. Singheiser, *Influence of mean stresses on fatigue life and damage of a turbine blade steel in the VHCF-regime.* Int J Fatigue 49 (2013) 90-99.